Nonlinear Dynamics **8:** 513–528, 1995.

Quasiperiodic Oscillations in Robot Dynamics

G. STÉPÁN
Department of Applied Mechanics, Technical University of Budapest, H-1521 Budapest, Hungary

and

G. HALLER
Division of Applied Mathematics, Brown University, Providence, RI 02912, U.S.A.

(Received: 15 May 1993; accepted: 26 September 1994)

Abstract. Delayed robot systems, even of low degree of freedom, can produce phenomena which are well understood in the theory of nonlinear dynamical systems, but hardly ever occur in simple mechanical models. To illustrate this, we analyze the delayed positioning of a single degree of freedom robot arm which leads to an infinite dimensional dynamical system. Restricting the dynamics to a four dimensional center manifold, we show that the system undergoes a codimension two Hopf bifurcation for an infinite set of parameter values. This provides a mechanism for the creation of two-tori in the phase space and gives a theoretical explanation for self-excited quasiperiodic oscillations of force controlled robots. We also compare our results with experimental data.

Key words: Codimension two bifurcation, force control, sampling, time delay.

1. Introduction

It is well known that force controlled robots tend to lose robustness or even stability depending on the environment they are in contact with. Since force disturbances, like the Coulomb friction, may cause large fluctuation in the contact force between the robot end effector and the environment (or workpiece), the application of great proportional control gains is necessary to reduce this error. However, large gains often cause instability. There are several proposed explanations for this type of instability at high gains, including, e.g., Craig [3], Asada and Slotine [2], and Vischer and Khatib [18]. In contrast to these studies, the experimental evidence presented in this paper suggests that the most important cause of instability is the effect of sampling time and the related delay in digital control. Without modeling these effects, one can neither give an accurate description of the loss of stability nor explain the appearance of nonlinear oscillations.

Continuous models, like those of An *et al.* [1] or Eppinger and Seering [4], can explain why force controlled robots tend to lose their stability more easily than their position controlled counterparts. At the same time, these models leave us without any conclusion for the optimal choice of sampling times. Whitney [19, 20] presents some analytical stability results for digital force control, but his models are too simple to account for the contact between the two basic vibratory systems: the soft force sensor and the environment. The simulation results of Kuno *et al.* [10] emphasize the possible destabilizing effect of sampling showing instability in force controlled robot systems at a sampling time near 0.1 ms. However, in many cases, e.g., for the experimental hybrid position/force controlled Newcastle robot studied in this paper, the sampling delay is substantially higher than this value. Only models including the effect of

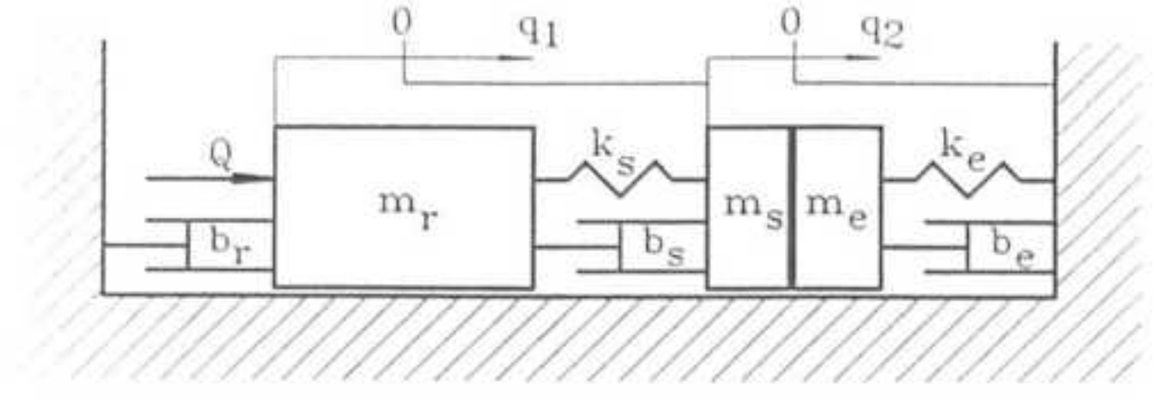

Fig. 1. Mechanical model of force control.

sampling were successful to explain the often unexpected stability properties of the Newcastle robot, which was originally designed for turbine blade polishing (Steven and Hewit [16]).

In this paper we study two robot systems which are closely related to the Newcastle robot mentioned above. First, we briefly discuss some experiments on a kinematically simplified version of the robot (single-axis force control in a limited domain of the workspace). We present stability charts constructed from experimental data and compare them with results obtained from a linear stability analysis of the system. We also discuss a truly nonlinear phenomenon, the occurrence of quasiperiodic oscillations with two or three frequencies slightly above the stability limit. We then propose a simple model which turns out to capture some of these nonlinear effects. This model contains time delay and admits a stability chart which has the same structure as that of the Newcastle robot. We study our infinite dimensional model using center manifold reduction, normal forms, and the methods of bifurcation theory to obtain closed form analytical results. These results indicate the existence of a two dimensional invariant torus and one or two limit cycles within a four dimensional center manifold in the infinite dimensional phase space of the model. These invariant manifolds in the model system explain the occurrence of quasiperiodic and periodic oscillations in the underlying physical system. We also present numerical results which confirm our analytical calculations. Finally, we discuss how more sophisticated modeling could explain the occurrence of stable three-frequency motions in real robot structures.

2. Stability Experiments on Digital Force Control

In order to obtain clearly arranged experimental results, we used a single-axis force control implementation of the hybrid controlled Newcastle robot and studied it only near a certain point of the workspace (see Stépán *et al.* [14] for details). Although the corresponding mechanical model describes only one DOF of the robot, it still has two mechanical degrees of freedom (see Figure 1) corresponding to the two general coordinates q_1 and q_2. Note that q_1 is the displacement of the first block relative to the second. The coordinates are zero when the spring forces are zero. The control force is denoted by Q, m refers to the mass, and b and k stand for the damping factor and stiffness, respectively. The subscripts r, s, and e refer to the robot manipulator, force sensor, and environment, respectively.

In practice, the manipulator inertia m_r is much greater than the inertia of the sensor m_s. The sensor damping b_s is also small compared to the manipulator damping b_r. The force sensor is soft (i.e., k_s is small) as suggested by Whitney [20] or Craig [3]. The dynamic behavior of a force controlled robot becomes fairly complicated when the environment is also an oscillatory system (see Figure 1) and this subsystem has a relatively low natural frequency $\sqrt{k_e/m_e}$ and slight damping b_e. Since the force sensor is in contact with the environment, the two blocks representing them appear through the joint inertia $m_s + m_e$ in the equations of motion. We

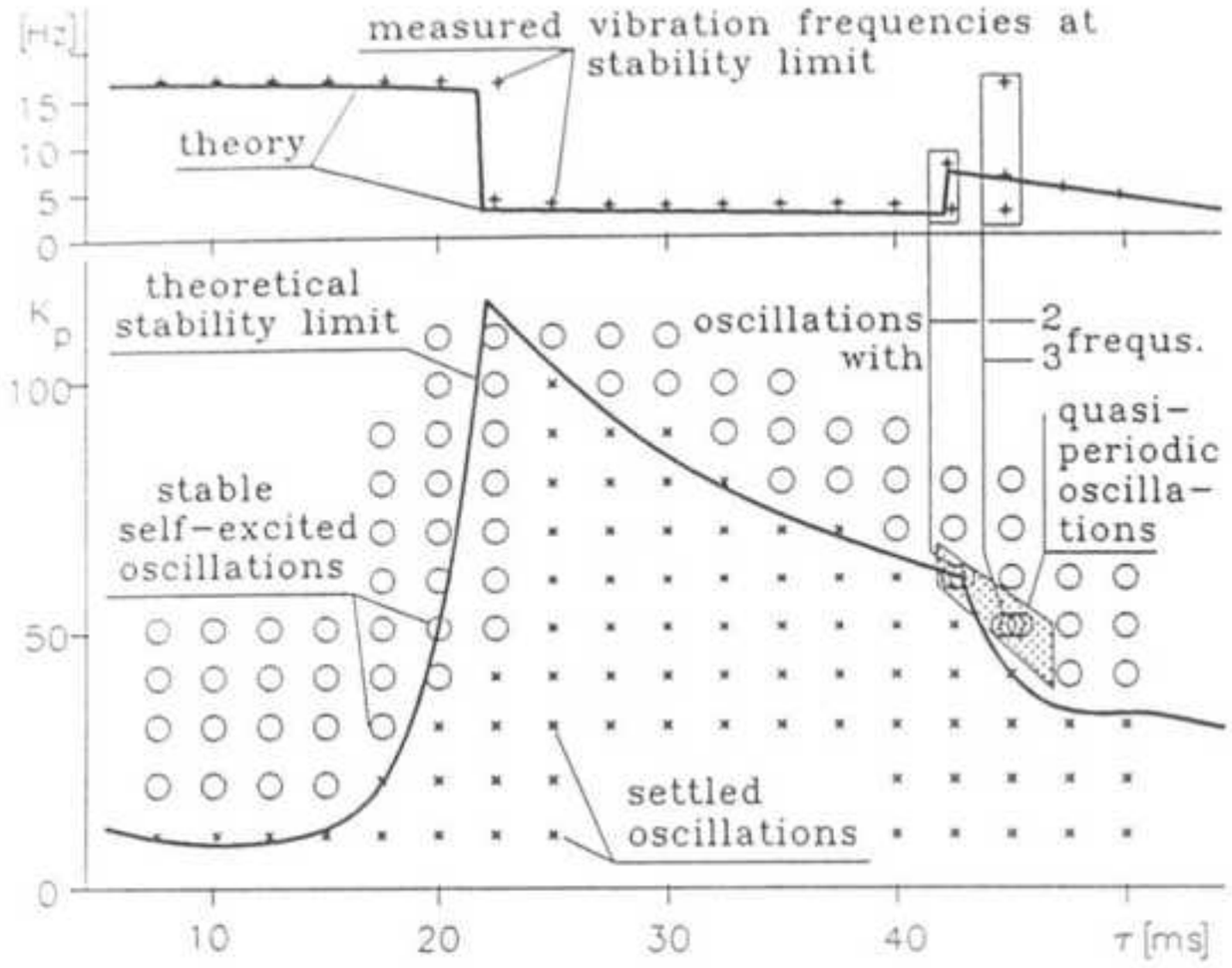

Fig. 2. Stability chart of force controlled robot.

experimentally identified the values of the mechanical parameters to find

$$m_r \approx 2500\,\text{kg}, \quad b_r \approx 32\,\text{Ns/mm},$$
$$m_s = 0.95\,\text{kg}, \quad b_s \approx 0.002\,\text{Ns/mm}, \quad k_s = 44.5\,\text{N/mm},$$
$$m_e = 4.43\,\text{kg}, \quad b_e \approx 0.0025\,\text{Ns/mm}, \quad k_e = 13.3\,\text{N/mm}.$$

Regarding these parameter values we note that the mass of the end effector is included in m_s and the relatively high value of the parameters m_r and b_r is due to the high gear ratio at a ball screw.

The above model can be thought of as the coupling of two 1 DOF subsystems. If $m_s + m_e \approx 0$, then the "manipulator subsystem" is a strongly overdamped system with a relative damping factor $\kappa_r = 3.16$. In case of $m_r \to \infty$, the "sensor/environment subsystem" is characterized by $\omega_{0s} = 103.7$ rad/s, $\kappa_s = 0.004$; hence it is a slightly damped oscillatory system with a natural frequency of about 16.5 Hz.

We will assume the control force in the form

$$Q(t) = K_p(F_d - k_s q_1(t_j - \tau)) + k_s q_1(t_j - \tau), \quad t \in [t_j, t_j + \tau) \quad j = 0, 1, \ldots \tag{1}$$

This agrees with the scheme suggested by Raibert and Craig [12] where the constant desired force

$$F_d = 50\,\text{N}$$

was set during the experiments. The sensed force is substituted as $F_s = k_s q_1$ using the sensor spring deformation q_1. There are only two parameters left which were actually varied in the stability experiments: the proportional gain K_p and the sampling time τ. With the latter one, the time of the jth sampling is $t_j = j\tau$.

The stability chart in the plane of these two parameters is presented in Figure 2. The robot was programmed to touch the environment, a steel cantilever beam, at a specified point of

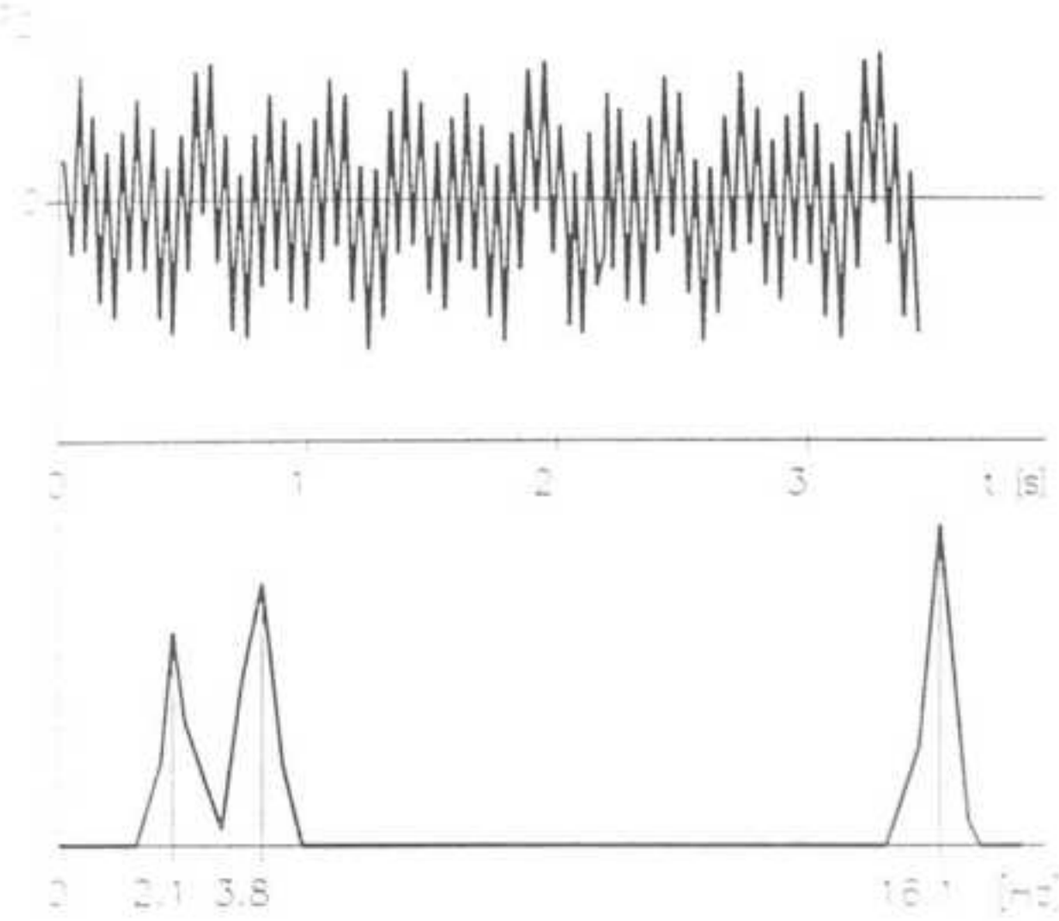

Fig. 3. Self-excited quasiperiodic oscillation and its spectrum: $\tau = 45$ [ms], $K_p = 50$.

the workspace. The crosses refer to parameter values for which the task was accomplished successfully, while the circles refer to self-excited vibrations which did not settle, i.e., the desired equilibrium of the robot was unstable. The frequencies of these oscillations along the stability limit are also shown above the stability chart.

Although we could not investigate cases of sampling times less than 6 ms with the processor we used, the peculiar structure of the stability region is possibly the same in that region, too. Our linear stability analysis also confirmed the experimental results, as shown by the continuous lines in Figure 2. To obtain these lines, we considered the linearized equations

$$\begin{pmatrix} m_r & m_r \\ m_r & m_r + m_s + m_e \end{pmatrix} \begin{pmatrix} \ddot{q}_1 \\ \ddot{q}_2 \end{pmatrix} + \begin{pmatrix} b_r + b_s & b_r \\ b_r & b_r + b_e \end{pmatrix} \begin{pmatrix} \dot{q}_1 \\ \dot{q}_2 \end{pmatrix} + \begin{pmatrix} k_s & 0 \\ 0 & k_e \end{pmatrix} \begin{pmatrix} q_1 \\ q_2 \end{pmatrix} = \begin{pmatrix} Q \\ Q \end{pmatrix}, \tag{2}$$

where Q is the same as in (1). The stability of the equilibrium

$$\begin{pmatrix} q_{10} \\ q_{20} \end{pmatrix} = \begin{pmatrix} F_d/k_s \\ F_d/k_e \end{pmatrix}$$

can be studied by transforming equations (1)–(2) into a five dimensional discrete mapping and applying Jury's criterion (Kuo [11]). An outline of this lengthy calculation is given in Stépán *et al.* [15] for a 1 DOF case.

We would like to draw attention to the self-excited quasiperiodic oscillations with two or even three different frequencies in the shaded domain of the parameter plane in the vicinity of a "corner" of the stability region. Figure 3 presents a typical time history of a vibration in that parameter region together with its spectrum, which clearly shows three distinct frequencies. All three frequencies are indicated above the stability chart in Figure 2, and they all have an obvious connection with the theoretical frequency lines determined from the linear theory.

However, the proof for the existence of these quasiperiodic oscillations as well as their analytical approximation require nonlinear methods. Following Takens [17], Guckenheimer

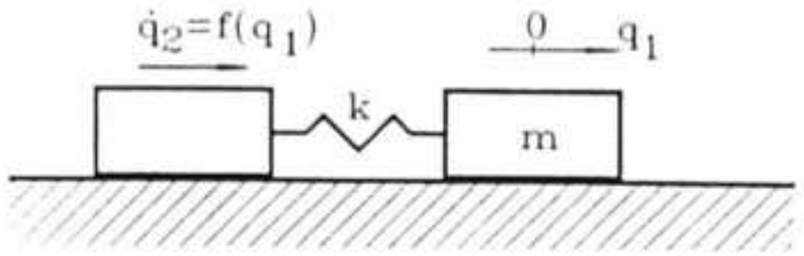

Fig. 4. Mechanical model of robot control via a kinematic constraint.

and Holmes [5] provide results from bifurcation theory in a form applicable to these problems, but the necessary calculations are rather complex and one usually has to appeal to some symbolic computation package to cope with them. In that case one has no direct control over the individual steps of the computations and special care must be taken to ensure the correctness of the symbolic code and the initial data (and the credibility of the results). As a first step in this program, we now present a similar but simpler model where closed form analytical calculations are possible without symbolic manipulations.

3. Nonlinear Analysis of Delayed Robot Control

Figure 4 shows a model of robot control through a kinematic constraint. An actuator provides the constrained velocity of the body on the left, and the position of the end-effector with mass m is measured by the coordinate q_1. The two bodies are connected by a flexible element of stiffness k. The damping is neglected to simplify the calculations. The equations of motion can be written as

$$\ddot{q}_1(t) + \omega_n^2(q_1(t) - q_2(t)) = 0, \quad \dot{q}_2 = g(q_1(t-\tau)), \tag{3}$$

where $\omega_n = \sqrt{k/m}$ is the natural frequency of the uncontrolled system (i.e., $\dot{q}_2 \equiv 0$) and the function g in the feedback is odd and C^3 smooth near the origin:

$$g(q_1) = -\chi q_1 + \varepsilon q_1^3 + \cdots. \tag{4}$$

If χ and ε are positive, this function is locally a good approximation for the saturation-like or degressive nonlinearity of the actuator. We assume a purely analog time delay τ in the control. The delay of an analog controller is somewhat different from the sampling time of a digital one, but its effect on the stability of the system is similar.

3.1. Linear Stability

First, we investigate the stability of the $q_1 = 0$ position. Let us introduce the nondimensionalized time letting $\tilde{t} := t/\tau$ and dropping the tilde immediately. The nondimensionalized delay T, the gain K, and the quality factor E will then read

$$T = \tau\omega_n, \quad K = \chi/\omega_n, \quad E = \varepsilon/\omega_n. \tag{5}$$

Up to cubic order, equation (3) of motion can be transformed into a three dimensional system for the new variable $\mathbf{x} = (x_1\ x_2\ x_3)^T = (q_1\ \dot{q}_1\ \ddot{q}_1)^T$ of the form

$$\dot{\mathbf{x}}(t) = \mathbf{L}\mathbf{x}(t) + \mathbf{R}\mathbf{x}(t-1) + \mathbf{f}(\mathbf{x}(t-1)), \tag{6}$$

where

$$\mathbf{L} = \begin{pmatrix} 0 & 1 & 0 \\ 0 & 0 & 1 \\ 0 & -T^2 & 0 \end{pmatrix}, \quad \mathbf{R} = \begin{pmatrix} 0 & 0 & 0 \\ 0 & 0 & 0 \\ -KT^3 & 0 & 0 \end{pmatrix}, \quad \mathbf{f}(\mathbf{x}) = \begin{pmatrix} 0 \\ 0 \\ ET x_1^3 \end{pmatrix}.$$

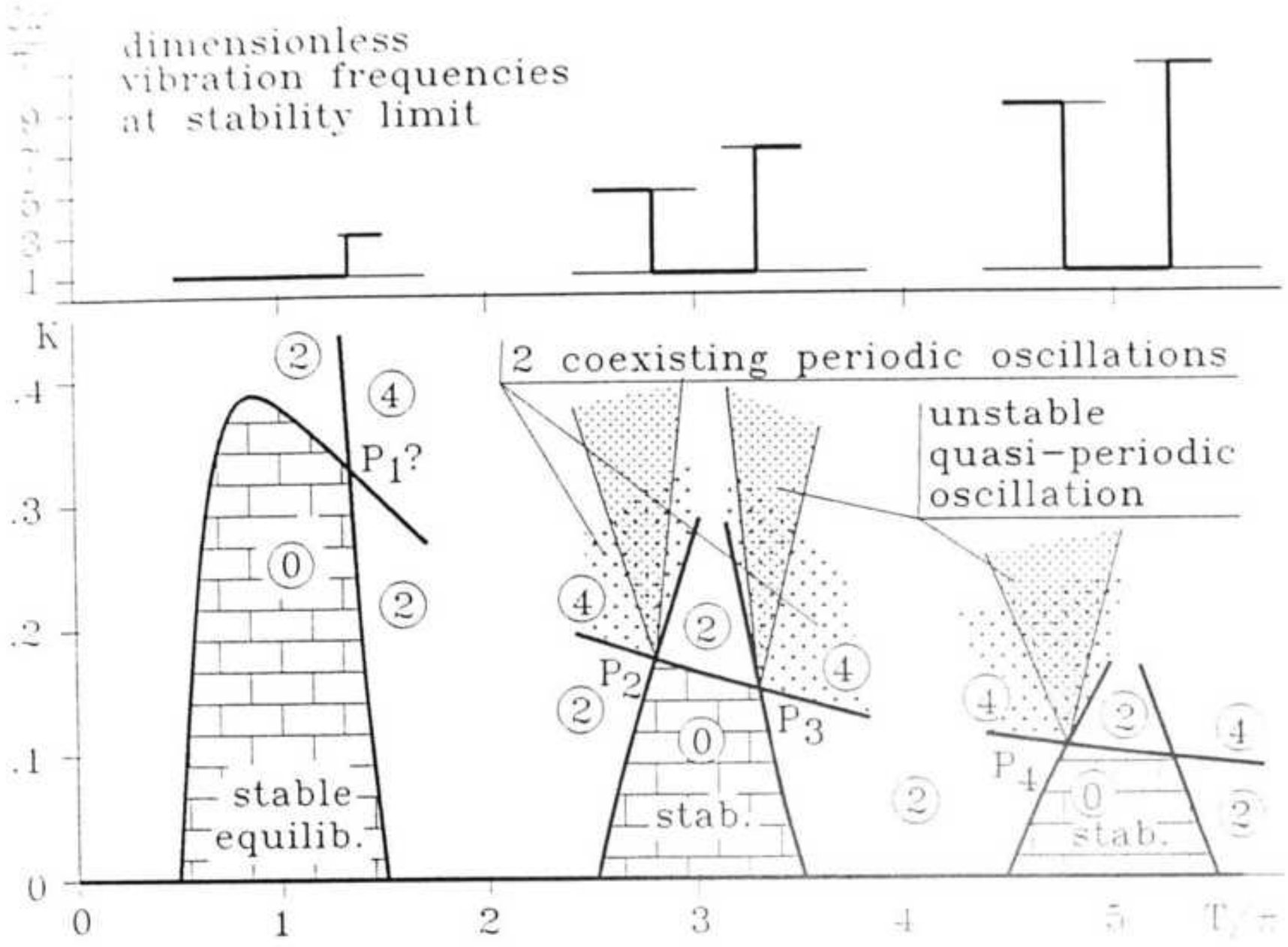

Fig. 5. Stability chart of delayed robot control.

The associated characteristic function is

$$D(\lambda, T, K) = \det(\lambda \mathbf{I} - \mathbf{L} - \mathbf{R}e^{-\lambda}) = \lambda^3 + T^2\lambda + KT^3e^{-\lambda}, \tag{7}$$

which is analyzed in Stépán [13] in detail. It turns out, that all the infinitely many characteristic roots λ_i of $D(\lambda, T, K)$ have negative real parts in the stability domains shown in Figure 5. The number of characteristic roots with positive real parts is also indicated by encircled numbers. The stability limits in the parameter plane (T, K) are given by

$$K_{(h)}(T) = (-1)^{h+1} \prod_{j=-1}^{1} \left(\frac{(2h+1)\pi}{2T} + j \right), \quad h = 0, 1, \ldots \tag{8}$$

which can be calculated using the D-subdivision method [13].

Note that the stability chart of system (3) in Figure 5 has a structure similar to the experimental stability diagram in Figure 2. In particular, one recovers the same "corner points" along the stability limit. They are denoted by P_k $(k = 1, 2, \ldots)$ (see Figure 5) and are located at the intersections (T_k, K_k) of the corresponding stability limit curves:

$$K_{(0)}(T) = K_{(k)}(T) \;\Rightarrow\; T_k = \sqrt{j_k}\,\frac{\pi}{2}, \quad K_k = \frac{j_k - 1}{\sqrt{j_k^3}},$$

$$j_k = 4k^2 + (2k+1)(2 + (-1)^k), \quad k = 1, 2, \ldots \tag{9}$$

At these points there are two pairs of pure imaginary characteristic roots and all the other roots have negative real parts:

$$\lambda_h, \bar{\lambda}_h = \pm i\omega_h = \pm i\left(\frac{\pi}{2} + h\pi\right), \quad h = 0, k; \quad \operatorname{Re}\lambda_j < 0, \quad j \neq 0, k. \tag{10}$$

The nondimensionalized vibration frequencies ω_h are also shown in Figure 5 above the stability chart.

It can be proved that for $E > 0$ supercritical Hopf bifurcations occur along the stability limits, which implies the existence of stable periodic oscillations in the system above these limits. Note, however, that quasiperiodic oscillations may also appear in some sectors of the parameter plane at the points P_k, where the linear analysis suggests Hopf bifurcations of codimension 2 (see (10) above). In the following we will focus our attention on the analysis of the system around these critical points.

3.2. Operator Differential Equation Formulation

Mathematically speaking, equation (6) is a retarded differential difference equation which can also be viewed as an infinite dimensional dynamical system. As it is shown in Hale [6] or Kuang [9], it can either be described in the form of a retarded functional differential equation

$$\dot{\mathbf{x}}(t) = \int_{-1}^{0} [\mathrm{d}\mathbf{A}(\vartheta)]\mathbf{x}(t+\vartheta) + \mathbf{f}(\mathbf{x}_t(-1)), \tag{11}$$

where $\mathbf{A}$ is a matrix function of bounded variation defined on the interval $[-1,0]$ by

$$\mathbf{A}(\vartheta) = \begin{cases} -\mathbf{R}, & \text{if } \vartheta = -1 \\ \mathbf{O}, & \text{if } \vartheta \in (-1,0) \\ \mathbf{L}, & \text{if } \vartheta = 0 \end{cases}, \tag{12}$$

or in the form of an operator differential equation

$$\dot{\mathbf{x}}_t = \mathcal{A}\mathbf{x}_t + \mathcal{F}(\mathbf{x}_t), \tag{13}$$

where the linear operator $\mathcal{A}$ and the nonlinear $\mathcal{F}$ act on the linear vector space $\mathcal{H}$ of continuously differentiable functions $u : [-1,0] \to \mathbf{C}^3$. In particular,

$$\begin{aligned} \mathcal{A}\mathbf{u}(\vartheta) &= \begin{cases} \frac{\mathrm{d}}{\mathrm{d}\vartheta}\,\mathbf{u}(\vartheta), & \text{if } \vartheta \in [-1,0) \\ \mathbf{L}\mathbf{u}(0) + \mathbf{R}\mathbf{u}(-1), & \text{if } \vartheta = 0 \end{cases}, \quad \mathbf{u} \in \mathcal{H}, \\ \mathcal{F}(\mathbf{u})(\vartheta) &= \begin{cases} \mathbf{O}, & \text{if } \vartheta \in [-1,0) \\ \mathbf{f}(\mathbf{u}(-1)), & \text{if } \vartheta = 0 \end{cases}. \end{aligned} \tag{14}$$

Both in equations (11) and (12), the function $\mathbf{x}_t \in \mathcal{H}$ is defined by the shift of time

$$\mathbf{x}_t(\vartheta) = \mathbf{x}(t+\vartheta), \quad \vartheta \in [-1,0].$$

We will also need the space $\mathcal{H}^*$ of continuously differentiable functions $\mathbf{v} : [0,1] \to \mathbf{C}^3$. We now define a bilinear form $(\ ,\ ) : \mathcal{H}^* \times \mathcal{H} \to R$ by

$$(\mathbf{v},\mathbf{u}) = \mathbf{v}^*(0)\mathbf{u}(0) + \int_{\vartheta=-1}^{0} \int_{\xi=\vartheta}^{0} \mathbf{v}^*(\xi-\vartheta)[\mathrm{d}\mathbf{A}(\vartheta)]\mathbf{u}(\xi)\,\mathrm{d}\xi, \quad \mathbf{u} \in \mathcal{H}, \mathbf{v} \in \mathcal{H}^*. \tag{15}$$

For the details of how this form arises naturally in the eigenfunction representation of system (13), see Hale [6].

3.3. Four Dimensional Center Manifold

As the analysis in Section 3 shows, in the neighborhoods of the points P_k of the parameter space the nonlinear stability of the fixed point $\mathbf{x}_t(\vartheta) \equiv 0$ is not determined by the eigenvalues of the linearized problem. (Simple calculation shows that the characteristic roots obtained in (10) in fact coincide with the eigenvalues of the operator $\mathcal{A}$.) As far as the true local nonlinear behavior is considered near the P_k's, Hopf bifurcations of codimension 2 can occur near the degenerate equilibria (see Guckenheimer and Holmes [5]). This phenomenon can be studied on a four dimensional center manifold embedded in the infinite dimensional phase space. A first order approximation to this center manifold is given by the center subspace of the associated linear problem, which is spanned by the corresponding infinite dimensional eigenvectors $\mathbf{s}_0$, $\bar{\mathbf{s}}_0$, $\mathbf{s}_k$, $\bar{\mathbf{s}}_k$ corresponding to the four critical characteristic roots in (10). This approximation is usually not adequate and one has to compute a second order Taylor-series expansion of the center manifold. However, the nonlinear terms in equation (3) have a discrete symmetry: they are invariant under the transformation $q \to -q$. As a result, the equations contain no quadratic terms which insures that the center subspace is a good approximation up to second order. This simplifies the calculations tremendously, as in other similar applications of center manifolds for delay-differential equations (see Stépán [13]).

In order to calculate the above-mentioned four eigenvectors of the operator $\mathcal{A}_{(k)}$ at the critical parameter point P_k, the matrices

$$\mathbf{L}_{(k)} = \begin{pmatrix} 0 & 1 & 0 \\ 0 & 0 & 1 \\ 0 & -j_k^2 \frac{\pi^2}{4} & 0 \end{pmatrix}, \quad \mathbf{R}_{(k)} = \begin{pmatrix} 0 & 0 & 0 \\ 0 & 0 & 0 \\ -(j_k - 1)\frac{\pi^3}{8} & 0 & 0 \end{pmatrix}, \tag{16}$$

have to be substituted into the definition (14) of $\mathcal{A}$ where the integer j_k is given as in formula (9). The eigenvectors satisfy

$$\mathcal{A}_{(k)}\mathbf{s}_h = \lambda_h \mathbf{s}_h, \quad h = 0, k.$$

In accordance with formulas (10), (14) and (16), this equation is equivalent to the linear boundary value problems

$$\frac{\mathrm{d}}{\mathrm{d}\vartheta}\,\mathbf{s}_h(\vartheta) = i(2h+1)\frac{\pi}{2}\,\mathbf{s}_h(\vartheta), \quad \vartheta \in [-1, 0),$$

$$\mathbf{L}_{(k)}\mathbf{s}_h(0) + \mathbf{R}_{(k)}\mathbf{s}_h(-1) = i(2h+1)\frac{\pi}{2}\,\mathbf{s}_h(0), \quad h = 0, k.$$

The solution functions

$$\mathbf{s}_h(\vartheta) = \begin{pmatrix} 1 \\ i(2h+1)\frac{\pi}{2} \\ -(2h+1)^2\frac{\pi^2}{4} \end{pmatrix} e^{i(2h+1)(\pi/2)\vartheta}, \quad h = 0, k \tag{17}$$

and their complex conjugates $\bar{\mathbf{s}}_h$, $h = 0, k$ give the critical right-hand eigenvectors of the operator $\mathcal{A}_{(k)}$. Its critical left-hand eigenvectors $\mathbf{n}_h$, $h = 0, k$ satisfy

$$\mathcal{A}^*_{(k)}\mathbf{n}_h = \bar{\lambda}_h \mathbf{n}_h, \quad h = 0, k,$$

where the adjoint operator $\mathbf{A}^*_{(k)}$ is defined by

$$\mathcal{A}^*_{(k)}\mathbf{v}(\psi) = \begin{cases} -\frac{\mathrm{d}}{\mathrm{d}\psi}\,\mathbf{v}(\psi), & \text{if } \psi \in (0,1] \\ \mathbf{L}^*_{(k)}\mathbf{v}(0) + \mathbf{R}^*_{(k)}\mathbf{v}(1), & \text{if } \psi = 0 \end{cases}, \quad \mathbf{v} \in \mathcal{H}^*.$$

The solutions of the corresponding boundary value problems assume the form

$$\mathbf{n}_h(\psi) = c_h \begin{pmatrix} (-1)^h \frac{j_k - 1}{2h+1}\,\frac{\pi^2}{4} \\ -i(2h+1)\frac{\pi}{2} \\ 1 \end{pmatrix} e^{i(2h+1)(\pi/2)\psi}, \quad h = 0, k, \tag{18}$$

where the complex numbers c_h, $h = 0, k$ come from the orthonormality conditions

$$(\mathbf{n}_l, \mathbf{s}_h)_{(k)} = \delta_{lh}, \quad l, h = 0, k. \tag{19}$$

The subscript k refers to the fact that $\mathcal{A}_{(k)}$ from (12) and (16) needs to be substituted in the bilinear form (15), and δ is the Kronecker symbol. For the case $l = h$, equation (19) assumes the form

$$\mathbf{n}^*_h(0)\mathbf{s}_h(0) - (j_k - 1)\frac{\pi^3}{8}\int_{-1}^{0} \bar{n}_{h3}(\xi + 1)s_{h1}(\xi)\,\mathrm{d}\xi = 1, \quad h = 0, k. \tag{20}$$

After substituting (17) and (18) into (20), one obtains the following expression for the complex coefficient in $\mathbf{n}_h$:

$$c_h = \frac{8}{\pi^2}\,\frac{2j_k - 6(2h+1)^2 + i(-1)^h(j_k - 1)\pi}{(2j_k - 6(2h+1)^2)^2 + (j_k - 1)^2\pi^2}, \quad h = 0, k. \tag{21}$$

Following Hale [6] and Hassard *et al.* [7], we now decompose the solution $\mathbf{x}_t(\vartheta)$ into components lying in the center subspace and components transverse to the center subspace. We let

$$\mathbf{x}_t(\vartheta) = \sum_{h=0,k} y_h(t)\mathbf{s}_h(\vartheta) + \sum_{h=0,k} \bar{y}_h(t)\bar{\mathbf{s}}_h(\vartheta) + \mathbf{w}(t)(\vartheta), \quad \vartheta \in [-1, 0], \quad t \in R,$$

where

$$y_h(t) = (\mathbf{n}_h, \mathbf{x}_t)_{(k)}, \quad h = 0, k$$

are the coordinates of $\mathbf{x}_t$ in the directions of $\mathbf{s}_h$, $h = 0, k$ (center subspace), and the infinite dimensional vector

$$\mathbf{w}(t) = \mathbf{x}_t - 2\mathrm{Re}\,(y_0(t)\mathbf{s}_0 + y_k(t)\mathbf{s}_k), \quad \mathbf{w}(t) \in \mathcal{H}$$

gives the remaining part of $\mathbf{x}_t$. We can write

$$\begin{aligned} \dot{y}_h(t) &= (\mathbf{n}_h, \dot{\mathbf{x}}_t)_{(k)} = (\mathcal{A}^*\mathbf{n}_h, \mathbf{x}_t)_{(k)} + (\mathbf{n}_h, \mathcal{F}(\mathbf{x}_t))_{(k)} \\ &= \lambda_h(\mathbf{n}_h, \mathbf{x}_t)_{(k)} + \mathbf{n}^*_h(0)\mathcal{F}(\mathbf{x}_t)(0) \\ &= i(2h+1)\frac{\pi}{2}\,y_h(t) + \bar{c}_h E\sqrt{j_k^3}\,\frac{\pi^3}{8} \\ &\quad \times (w_1(t)(-1) + 2\mathrm{Re}\,(y_0(t)s_{01}(-1) + y_k(t)s_{k1}(-1)))^3. \end{aligned}$$

This yields the transformed system of differential equations

$$\begin{pmatrix} \dot{y}_0 \\ \dot{y}_k \\ \dot{\mathbf{w}} \end{pmatrix} = \begin{pmatrix} i\frac{\pi}{2} & 0 & 0 \\ 0 & i(2k+1)\frac{\pi}{2} & 0 \\ 0 & 0 & \mathcal{A} \end{pmatrix} \begin{pmatrix} y_0 \\ y_k \\ \mathbf{w} \end{pmatrix} + \begin{pmatrix} \bar{c}_0 E\sqrt{j_k^3}\,\frac{\pi^3}{8}\,(w_1(-1) + 2\mathrm{Im}\,(y_0 + (-1)^k y_k))^3 + \text{h.o.t.} \\ \bar{c}_k E\sqrt{j_k^3}\,\frac{\pi^3}{8}\,(w_1(-1) + 2\mathrm{Im}\,(y_0 + (-1)^k y_k))^3 + \text{h.o.t.} \\ \text{h.o.t.} \end{pmatrix},$$

where h.o.t. stands for higher order terms of no importance later, and the corresponding equations for $\bar{y}_0$ and $\bar{y}_k$ has been omitted to simplify formulation.

As explained above, the above system has a four dimensional center manifold which is tangent to the four dimensional $(y_0, \bar{y}_0, y_k, \bar{y}_k)$ plane. In our new coordinates, it assumes the form

$$\mathbf{w} = \mathcal{O}(|y_0|^2, |y_k|^2).$$

This shows that using the complex variables

$$z_1 = y_0, \quad z_2 = y_k,$$

the cubic truncation of system (6) restricted to its center manifold at P_k can be cast in the form

$$\dot{z}_1 = i\omega_0 z_1 + i\bar{c}_0 E\sqrt{j_k^3}\,\frac{\pi^3}{8}\,(z_1 - \bar{z}_1 + (-1)^k(z_2 - \bar{z}_2))^3, \tag{22a}$$

$$\dot{z}_2 = i\omega_k z_2 + i\bar{c}_k E\sqrt{j_k^3}\,\frac{\pi^3}{8}\,(z_1 - \bar{z}_1 + (-1)^k(z_2 - \bar{z}_2))^3. \tag{22b}$$

The corresponding two conjugate equations complete the four dimensional system.

3.4. Normal Form

To simplify the analysis of the equations (22a–b) on the center manifold, one can put these equations in normal form through a further near-identity change of variables (see, e.g., Guckenheimer and Holmes [5]). The corresponding normal form in the case of two pairs of pure imaginary eigenvalues was first derived by Takens [17] and later studied by Guckenheimer and Holmes [5] in more detail. We use the basic normal form of Takens [17] without the standard simplifying transformations used in [5] and [17] to reduce the number of parameters. This way, we have two more terms in our normal form but we obtain the results directly in terms of the physical parameters of the problem.

Let us introduce the bifurcation parameters

$$\mu_1 = T - T_k, \quad \mu_2 = K - K_k \tag{23}$$

at the kth critical point P_k where $k = 2, 3, \ldots$ As shown in Takens [17], for small values of μ_1 and μ_2 the dynamics of system (22) near the origin is described by the truncated normal

form

$$\dot{r}_1 = r_1(b_{11}\mu_1 + b_{12}\mu_2 + a_{11}r_1^2 + a_{12}r_2^2), \tag{24a}$$

$$\dot{r}_2 = r_2(b_{21}\mu_1 + b_{22}\mu_2 + a_{21}r_1^2 + a_{22}r_2^2), \tag{24b}$$

$$\dot{\varphi}_1 = \omega_0 + \mathcal{O}(|r|)^2, \tag{24c}$$

$$\dot{\varphi}_2 = \omega_k + \mathcal{O}(|r|)^2, \tag{24d}$$

where the polar coordinates $r_1, r_2, \varphi_1, \varphi_2$ are related to our previous complex variables by the transformation $z_j = r_j e^{i\varphi_j}$, $j = 1, 2$. This normal form is only valid for nonresonant cases which means

$$m_1\omega_0 + m_2\omega_k \neq 0$$

holds for all possible nonzero integers m_1, m_2 satisfying $|m_1| + |m_2| \leq 4$. As one can see from (10), this nonresonance condition is violated for $k = 1$ when a 1:3 resonance occurs. Here we do not deal with this resonant case, and will assume that $k > 1$ holds.

The coefficients b_{ij} are just the derivatives of the critical characteristic roots with regard to the bifurcation parameters:

$$b_{1j} = \left.\frac{\partial\lambda_0}{\partial\mu_j}\right|_{\mu_1=\mu_2=0}, \quad b_{2j} = \left.\frac{\partial\lambda_k}{\partial\mu_j}\right|_{\mu_1=\mu_2=0}, \quad (j = 1, 2).$$

This calculation can be carried out via the implicit differentiation of the characteristic function (7) with regard to T and K, which (upon substitution of the critical parameter values T_k, K_k $(k = 2, 3, \ldots)$) yields

$$b_{11} = \frac{(j_k - 1)\pi}{\sqrt{j_k}} \frac{2(j_k - 3)}{4(j_k - 3)^2 + (j_k - 1)^2\pi^2}; \quad b_{12} = \frac{\sqrt{j_k^3}\,(j_k - 1)\pi^2}{4(j_k - 3)^2 + (j_k - 1)^2\pi^2};$$

$$b_{21} = \frac{(j_k - 1)\pi}{\sqrt{j_k}} \frac{6(j_k - 1) - 4(-1)^k j_k(2k + 1)}{(2j_k - 6(2k + 1)^2)^2 + (j_k - 1)^2\pi^2};$$

$$b_{22} = \frac{\sqrt{j_k^3}\,(j_k - 1)\pi^2}{(2j_k - 6(2k + 1)^2)^2 + (j_k - 1)^2\pi^2}.$$

To obtain the coefficients a_{ij} usually takes a vast amount of calculation. First, one has to compute the coefficients in the Taylor series of a near identity transformation which puts system (22) to the normal form (24), then obtain the coefficients in (24) as functions of the Taylor coefficients of system (22). Due to the symmetry of the nonlinearity in this problem, there are no quadratic terms in the Taylor expansion of the right-hand side of system (22). As a result, the cubic terms in the normal form (24) are exactly the corresponding cubic terms in system (22). Namely, we have

$$2a_{11} = a_{12} = -6E\sqrt{j_k^3}\,\frac{\pi^3}{8}\,\mathrm{Im}\,c_0; \quad a_{21} = 2a_{22} = (-1)^{k+1}6E\sqrt{j_k^3}\,\frac{\pi^3}{8}\,\mathrm{Im}\,c_k,$$

where c_0, c_k must be substituted from (21).

3.5. Analysis of the Truncated Normal Form

A quasiperiodic solution of system (24) with frequencies close to ω_0 and ω_k manifests itself as a fixed point (r_{100}, r_{200}) of equations (24a–b) (with $r_{j00} > 0$), which must satisfy

$$\begin{pmatrix} r_{100}^2 \\ r_{200}^2 \end{pmatrix} = -\begin{pmatrix} a_{11} & a_{12} \\ a_{21} & a_{22} \end{pmatrix}^{-1} \begin{pmatrix} b_{11} & b_{12} \\ b_{21} & b_{22} \end{pmatrix} \begin{pmatrix} \mu_1 \\ \mu_2 \end{pmatrix},$$

or, equivalently,

$$r_{100} = \frac{1}{3j_k\sqrt{E}} \sqrt{((5j_k - 3) - 4(-1)^k(2k+1)j_k)\frac{2}{\pi}\mu_1 + j_k^2\mu_2}\,, \tag{25a}$$

$$r_{200} = \frac{1}{3j_k\sqrt{E}} \sqrt{(-(j_k + 3) + 2(-1)^k(2k+1)j_k)\frac{2}{\pi}\mu_1 + j_k^2\mu_2}\,, \tag{25b}$$

for $k = 2, 3, \ldots$ and for positive quality factor E. Equations (25) define an invariant torus in the phase space of equations (24) provided

$$\mu_2 > \mu_1 \frac{2}{\pi j_k^2} \max\{-(5j_k - 3) - 4(-1)^k(2k+1)j_k, (j_k + 3) - 2(-1)^k(2k+1)j_k\}, \tag{26}$$

which defines a sector in the parameter plane for each $k \geq 2$ emanating from the point P_k. We have drawn these sectors in the stability chart of Figure 5 for $k = 2, 3, 4$. In case of P_2, the numerical values in (9) are as follows:

$$k = 2, \quad j_2 = 31, \quad T_2 = 2\sqrt{31}/\pi, \quad K_2 = 30\sqrt{31^3}$$

and the sector in question is given by

$$K - K_2 > \frac{936}{961\pi}(T - T_2) \quad \text{and} \quad K - K_2 > -\frac{552}{961\pi}(T - T_2).$$

Clearly, the dynamics on the invariant torus (25) is described by equations (24c–d). Therefore, the frequencies of the motion on the torus are $\mathcal{O}((r_{100}, r_{200})^2)$ close to the frequencies of a $1 : (2k+1)$-resonant torus. Generally, a $1 : (2k+1)$-resonant torus is filled with periodic orbits and the higher the value of k the longer the common period of these orbits is. Hence we can conclude that the higher the index of a given "corner point" P_k the more aperiodic the motion on our two-torus appears in numerical experiments. Whether the motion on the invariant torus we found in (25) is *actually* quasiperiodic or periodic depends on the values of the parameters (since r_{100} and r_{200} depend on the parameters, too). One can easily see that for almost all values of the parameters k, E, μ_1, and μ_2 the right-hand sides of equations (24c) and (24d) will be rationally independent. In other words, with the exception of the parameter values falling in a measure zero everywhere dense subset of the sector (26), the invariant torus (25) of the truncated normal form (24) will contain quasiperiodic trajectories. Even if we happen to pick parameters from the measure zero "resonant set", the corresponding periodic motions on the torus will look more and more aperiodic as we increase k. All these properties are clearly inherited by system (22) and our original model system (3) provided the torus we found is structurally stable. To check this one has to check the stability type of the torus. The linearization of the two dimensional subsystem (24a–b) around the fixed point (r_{100}, r_{200})

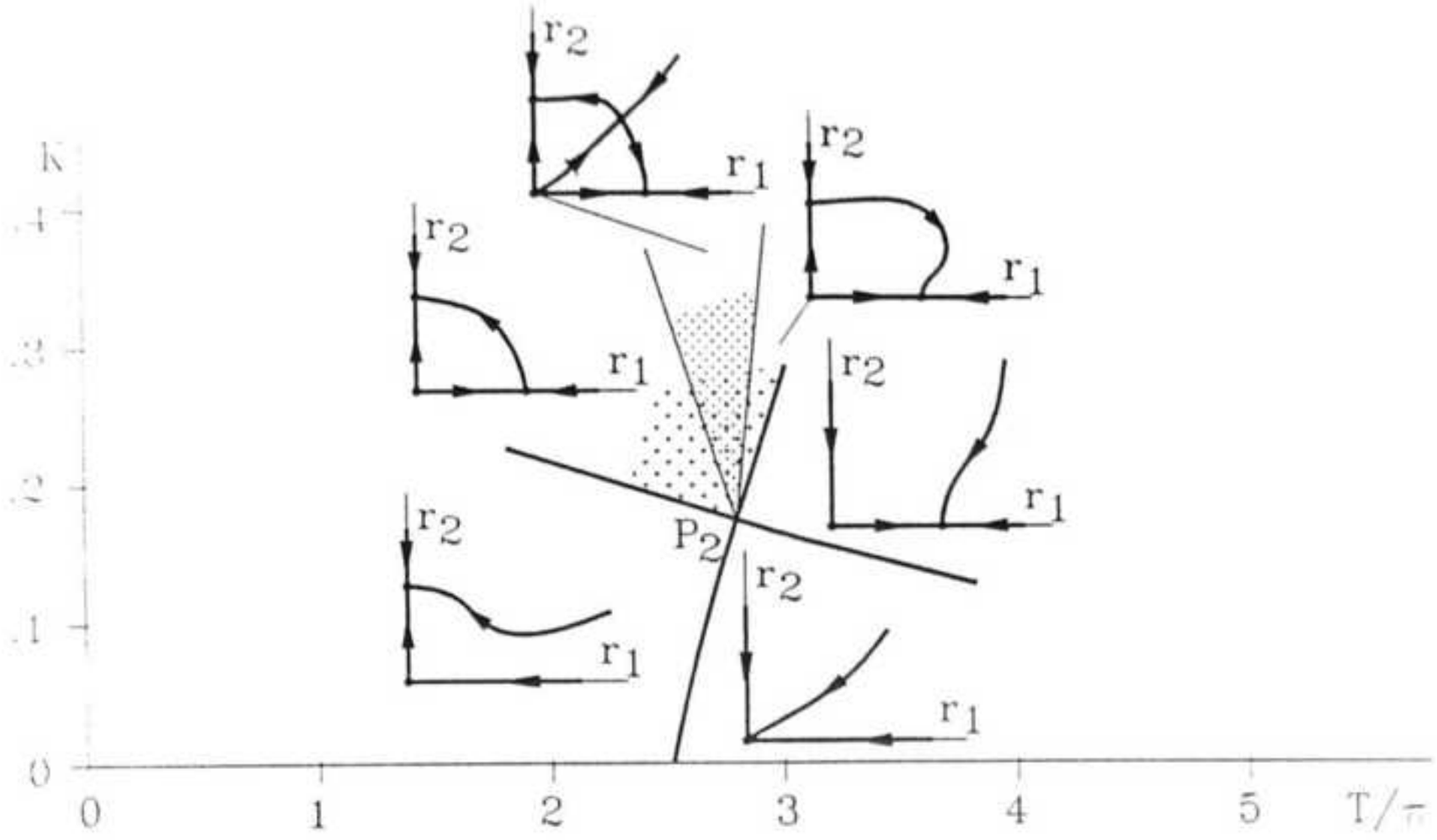

Fig. 6. The unfolding at P_2.

shows that these points in the (r_1, r_2) plane are of saddle type, i.e. the corresponding invariant torus is normally hyperbolic. One can show (see, e.g., Iooss and Mielke [8]), that for most parameter values the strength of this hyperbolicity is enough to ensure the preservation of the invariant torus under the effect of the "tail" of the normal form. Unfortunately, the periodic or quasiperiodic trajectories on the persisting tori are all (orbitally) unstable. One can, however, also look for periodic solutions for system (24) of the form $(r_1, r_2) = (r_{10}, 0)$ or $(r_1, r_2) = (0, r_{20})$ with frequencies close to ω_0 or ω_k, respectively. Straightforward calculations show that there are always two stable limit cycles of these types coexisting with the unstable invariant torus.

The full unfolding of the system (24a–b) at P_2 is presented in Figure 6. The points lying on the r_1 and r_2 axes represent the limit cycles, the point in the positive quadrant refers to the torus. These orbits also survive in system (3) together with the three dimensional heteroclinic manifolds connecting them to the torus. The reason for this is that the limit cycles have open domains of attraction and the two branches of the unstable manifold of the torus still intersect this domain under the effect of higher order terms. For similar reasons the heteroclinic connection between the unstable equilibrium and the two-torus also survives the effect of higher order terms. As a result, the stable and unstable manifolds of the persisting invariant torus keep acting as natural boundaries of domains of attraction, and separate the phase space into regions with different asymptotic behaviors.

As a verification of these results, Figure 7 shows the projection of some numerical solutions from the four dimensional center manifold onto a three dimensional coordinate space. The unstable torus is plotted based on the value of (r_{100}, r_{200}) calculated from (25) (after a transformation back into the real phase space of equations (22)). The two limit cycles are also obtained from our analytical calculations. The two solutions approaching the corresponding limit cycles are produced by numerical simulation. Undoubtedly, the simulation shows good agreement between the real dynamics of system (22) and the bifurcating objects calculated from the normal form (24).

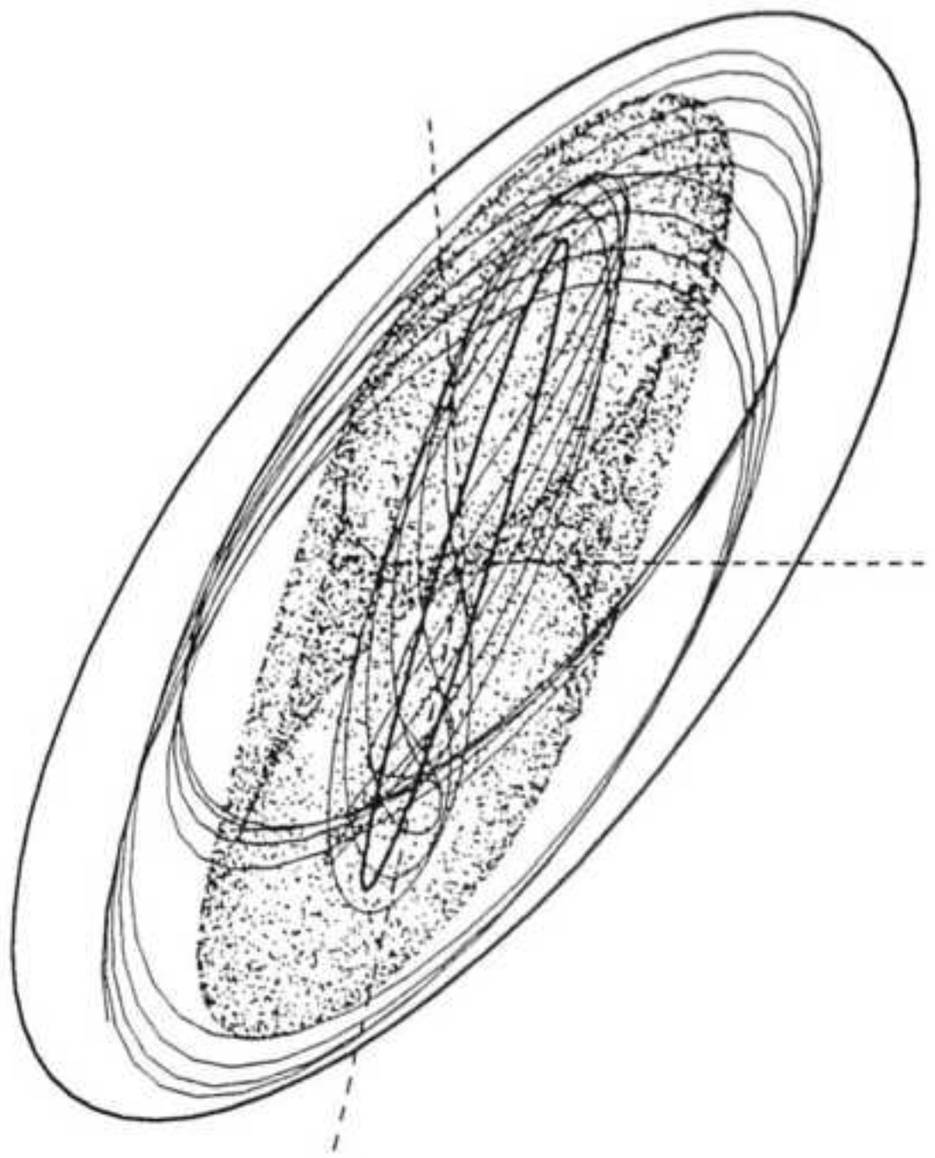

Fig. 7. Trajectories projected from the center manifold.

4. Conclusions

The nonlinear vibration analysis of this simplified delayed robot control was motivated by some experiments on a digitally controlled robot. The stability charts in Figures 2 and 5 (related to the systems in Figures 1 and 4, respectively) display the same structure in the plane of parameters. In both cases these parameters have the same physical meaning: they characterize the sampling time or time delay, and the proportional gain. The models are also similar in the sense that they both contain past effects and slightly damped oscillators.

As we noted earlier, the stability charts have critical points where self-excited quasiperiodic oscillations may occur. In both cases, these vibrations generically exist, but there are important qualitative differences between them:

- Experiments on force control: the (apparently) quasiperiodic oscillations are stable (surviving for a long period of time shown in Figure 3). They appear in a sector close to the stability limit (see the shaded region in Figure 2), and have either two or three characteristic frequencies.
- Analytical and numerical investigation of simplified delayed system: the quasiperiodic oscillations exist for almost all values of the parameters (in a measure-theoretical sense) and are unstable (see the unfolding in Figure 6). They appear in a sector opposite to the stability domain (see the shaded region in Figure 5), and contain motions with only two basic frequencies.

At this point, we have not yet carried out a similar bifurcation analysis for more sophisticated models of the real force-controlled robot. However, we can give an explanation for the partial discrepancy (discussed above) between our results and experiments. It is very likely that unstable quasiperiodic oscillations also exist in case of a force controlled robot, but they are hard to detect in experiments. Stable quasiperiodic oscillations do not exist in our simplified delayed system because the nonlinearity we considered is symmetric (see equation (4)).

For a real force controlled robot the saturation at the actuators is typically described by some asymmetric nonlinearity since the equilibrium in question is at $\mathbf{q}_0$ where the actuators are under load (see equation (2)). Thus, second order terms should also be included in the power series of the nonlinearity which would break the discrete symmetry of the model and would create a situation which is richer as far as possible bifurcations are concerned. Research in progress suggests that if one does include symmetry breaking quadratic terms in the analysis, the normal form (24) will admit stable invariant two-tori for a large set of parameter values.

Using an asymmetric model we also hope to be able to explain the three-frequency motions observed in the experiments. As it is shown by Guckenheimer and Holmes [5], the point (τ_{100}, τ_{200}) (see the unfolding in Figure 6) may undergo a Hopf bifurcation as the parameters are varied, which means the creation of a three-torus in the phase space of system (22).

We believe that these experimental and theoretical results highlight the complexity of force-controlled robot systems and show that the understanding of the underlying nonlinear dynamics cannot be complete without the implementation of the sample time and delay in our models.

Acknowledgements

The authors acknowledge the support of the Hungarian Scientific Foundation OTKA 5-328 and the Science and Engineering Research Council (U.K.). The authors would like to thank P. Brunowsky for useful discussions and for pointing out an error in an earlier manuscript.

References

1. An, C. H., Atkeson, C. G., and Hollerbach, J. M., 'Model-based control of a direct drive alarm. Part II: Control', in *Proceedings, IEEE Conference on Robotics and Automation*, Philadelphia, Pennsylvania, 1988, pp. 1386–1391.
2. Asada, H. and Slotine, J.-J., E., *Robot Analysis and Control*, Wiley, New York, 1986.
3. Craig, J. J., *Introduction to Robotics Mechanics and Control*, Addison-Wesley, Reading, Pennsylvania, 1986.
4. Eppinger, D. S. and Seering, W. P., 'Understanding bandwidth limitations in robot force control', in *Proceedings, IEEE Conference on Robotics and Automation*, Raleigh, North Carolina, 1987, pp. 904–909.
5. Guckenheimer, J. and Holmes, P., *Nonlinear Oscillations, Dynamical Systems, and Bifurcations of Vector Fields*, Springer-Verlag, New York, 1986.
6. Hale, J. K., *Theory of Functional Differential Equations*, Springer-Verlag, New York, 1977.
7. Hassard, B. D., Kazarinoff, D., and Wan, Y. H., *Theory and Applications of Hopf Bifurcations*, London Mathematical Society Lecture Note Series, Vol. 41, Cambridge, England, 1981.
8. Iooss, G. and Mielke, A., 'Bifurcating time-periodic solutions of Navier–Stokes equations in infinite cylinders', *Journal of Nonlinear Science* **1**, 1991, 107–146.
9. Kuang, Y., *Delay Differential Equations*, Academic Press, New York, 1993.
10. Kuno, T., Koide, M., Mimura, N., and Miyaguchi, H., 'Simulation analysis for force control six-joint manipulator', in *Proceedings, 4th International Symposium on Robotics Research*, Cambridge, England, 1988, pp. 207–216.
11. Kuo, B. C., *Digital Control Systems*, SRL Publishing Company, Champaign, Illinois, 1977.
12. Raibert, M. H. and Craig, J. J., 'Hybrid position/force control for computer controlled manipulators', *ASME Journal of Dynamic Systems, Measurement and Control* **102**, 1981, 125–133.
13. Stépán, G., *Retarded Dynamical Systems*, Longman, Harlow, England, 1989.
14. Stépán, G., Steven, A., and Maunder, L., 'Design principles of digitally controlled robots', *Mechanism and Machine Theory* **25**, 1990, 515–527.
15. Stépán, G., Steven, A., and Maunder, L., 'Theoretical and experimental stability analysis of a hybrid position-force controlled robot', in *Proceedings, 8th Symposium on Theory and Practice of Robots and Manipulators*, Cracow, Poland, 1990, pp. 53–60.
16. Steven, A. and Hewit, J. R., 'Hybrid position and force control applied to robotic polishing of turbine blading', in *Proceedings, ICAR'87 3rd Conference on Advanced Robotics*, Versailles, France, 1987, pp. 493–502.

17. Takens, F., 'Singularities of vector fields', *Publications Mathématiques, Institut des Hautes Etudes Scientifiques* **43**, 1974, 47–100.
18. Vischer, D. and Khatib, O., 'Design and development of torque-controlled joints', in *Experimental Robotics I*, V. Hayward and O. Khatib (eds.), Springer-Verlag, Berlin, Germany, 1990.
19. Whitney, D. E., 'Forced feedback control of manipulator fine motions', *ASME Journal of Dynamic Systems, Measurement and Control* **98**, 1977, 91–97.
20. Whitney, D. E., 'Historical perspective and state of the art in robot force control', *International Journal of Robotics Research* **6**, 1985, 3–14.